Theoretical investigation of the ELNES of transition metal carbides for the extraction of structural and bonding information

Andrew J. Scott and Rik Brydson
Department of Materials, School of Process, Environmental and Materials Engineering, University of Leeds, Leeds, LS2 9JT, United Kingdom

Maureen MacKenzie and Alan J. Craven
Department of Physics and Astronomy, University of Glasgow, Glasgow, G12 8QQ, United Kingdom
(Received 2 June 2000; revised manuscript received 18 October 2000; published 1 June 2001)

We present the results of theoretical modeling studies of the electron energy loss near-edge structure (ELNES) of Group-IVA (Ti, Zr, Hf) and Group-VA (V, Nb, Ta) transition-metal carbides exhibiting a cubic NaCl structure. Calculations of the unoccupied densities of states at both metal and nonmetal sites have been performed using both multiple scattering (MS) and full linearized-augmented-plane-wave (FLAPW) band-structure calculations. The effects of self-consistency and the inclusion of the core hole produced during the ELNES excitation process have been investigated for the case of the MS calculations, while the size of the basis set and the effect of charge transfer have been examined for the case of the FLAPW calculations. The results are compared to high-energy-resolution ELNES measurements. We demonstrate the sensitivity of ELNES features to quantities such as the lattice parameter, chemical composition, and stoichiometry.

DOI: 10.1103/PhysRevB.63.245105 PACS number(s): 71.20.−b, 71.15.Mb, 82.80.Pv, 68.37.Lp

I. INTRODUCTION

Transition-metal (TM) carbides are an important class of materials. They are unusual in possessing high melting points, extreme hardness, and electrical and thermal conductivities similar to those of the pure transition metals.[1] The early transition-metal carbides studied here have a cubic sodium chloride structure, and are able to exist over a range of compositions MC_x with $0.5<x<1.0$.[2]

TM carbides are employed as both single, multilayered, or graded coatings which are both hard and inert, and can exist as complex solid solutions with varying compositions and morphologies, depending on deposition and processing conditions.[3,4] A further engineering application of such materials lies in the precipitation strengthening, via dislocation pinning, of microalloyed steels. Here, complex mixed metal TM carbides, nitrides, and carbonitrides of varying stoichiometry, as well as duplex particles of nanometer dimensions, can all be present within a microalloyed steel structure.[5] The precipitation mechanisms and kinetics of such complex particles and their dependence on processing (heat treatment, rolling, etc.), including their behavior in the heat-affected zone produced during welding, are of prime importance if an accurate modeling of processing-property relationships and the consequent prediction of the remanent life of steel structures is to be achieved.

A parallel electron-energy-loss (EELS) spectrometer combined with a field-emission conventional or scanning transmission electron microscope (CTEM/STEM) enables high-energy-resolution electron-energy-loss near-edge structure (ELNES) measurements to be made at nanometer spatial resolution.[6] ELNES measurements probe the local unoccupied electronic structure in a solid. The technique therefore allows us to investigate localized changes in chemistry, structure, and bonding on a scale ideal for the study of nanocrystalline or nanostructured coatings and nanometer-sized precipitates of materials such as TM carbides. Further benefits of the high spatial resolution associated with EELS include the ability to interrogate grain boundaries, interfaces, and defects.[7]

Many theoretical studies have been conducted on TM carbides, concentrating on TiC in particular.[8–12] The influence of vacancies on these materials has also been examined.[13–15] These electronic band-structure calculations have been directed at understanding the fundamental bonding and properties of these materials. Bonding in these materials is dominated by strong covalent bonding between the metal and nonmetal; their band structures show a hybridization between the metal *d* states and the nonmetal *p* states. Although there is little metal-metal bonding in the carbides, this becomes more significant for the TM nitrides and substoichiometric materials, but at the expense of the metal-nonmetal interaction. Further electronic structure calculations of these materials will be presented in this work. However, we will concentrate mainly on the unoccupied states above the Fermi energy as these are most relevant for the analysis of ELNES data.

Significant ELNES data on the TM carbides has already been reported.[16] Complex ELNES, particularly for the nonmetallic element, are observed. This work presents theoretical electronic structure calculations specifically aimed at modeling experimental ELNES spectra from these materials and at ultimately increasing our comprehension of their material behavior and properties at the scale of nanometers.

Techniques for modeling ELNES from bulk crystalline materials are relatively well established. These methods are based on density-functional theory within the local-density approximation (LDA). However, many previously published band-structure calculations have not provided the necessary site and symmetry projections of the total unoccupied density of states (DOS) required for a comparison with experimental ELNES data. Furthermore, restrictions in computing

TABLE I. Muffin-tin sphere radii (a.u.) employed in the MS calculations of the TM carbides.

	ICXANES		FEFF8	
	Metal (a.u.)	Nonmetal (a.u.)	Metal (a.u.)	Nonmetal (a.u.)
TiC	2.2046	1.8848	2.5625	2.0787
VC	2.0510	1.8848	2.4491	2.0182
ZrC	2.4600	1.9793	2.8761	2.1184
NbC	2.3046	1.9196	2.6861	2.0730
HfC	2.4522	1.9348	2.8421	2.0938
TaC	2.2750	1.9348	2.7131	2.0182

power have limited these studies to relatively simple systems, and have not incorporated any effects due to the EELS excitation process. Consequently, in many previous studies, non-self-consistent cluster-based methods have been employed for the interpretation of EELS and X-ray-absorption near-edge structure (XANES) data.

With this in mind, the purpose of this work is to present a comparison of previous methods with those currently available, albeit on systems possessing a relatively high-symmetry structure. Although LDA-based methods are expected to provide accurate total energies, there is no *a priori* guarantee that they will efficiently describe the distribution of unoccupied states probed by the excited electron in EELS.

For this work we have employed a number of methods: the full linearized augmented plane wave (FLAPW) band-structure method as well as two differing methods based upon the multiple-scattering (MS) cluster based approach. We critically compare the results obtained from a number of publically available software packages. However, the ability to model ELNES should not necessarily be an end in itself—deeper understanding of the origin of ELNES features in terms of structural and bonding parameters within a solid is required. We have attempted to undertake this for the cubic TM carbides, and indicate how various ELNES features depend on quantities such as lattice parameter, chemical composition, and stoichiometry.

II. MODELING METHODS

A. Multiple scattering (MS)

The multiple-scattering calculations were performed using the XANES code of Pendry, Durham, and co-workers.[17,18] The multiple-scattering technique is based on the theory of interference between the outgoing electron wave, created by the ionization of an inner-shell electron, and the returning wave which has been elastically backscattered by the surrounding atoms in the solid. Scattering phase shifts and atomic matrix elements were calculated using a modified version of the Pendry MUFPOT code[19] based on the superposition of neutral atom potentials within the muffin tin approximation (phase shifts are based on a non-self-consistent calculation). The muffin-tin radii were chosen so as to minimize potential discontinuities at the boundary between individual muffin tins and to be nonoverlapping (Table I). For our calculations we have used a maximum angular momentum for the atomic phase shifts ($L_{\max}$) of 3, and a maximum angular momentum for the symmetrized expansion (L_{out}) of 11. L_{out} describes how the complex interference pattern is expanded about the central atom. The multiple-scattering calculation is performed in real space by dividing a cluster into concentric shells of atoms surrounding the central absorbing atom. Multiple scattering is solved first within each shell (intrashell), then between each shell (intershell) before the results are combined. For the TM carbides, convergence was generally achieved after the addition of seven shells out to a radius of approximately 0.6 nm, the cluster containing a total of 93 atoms. The effect of the core hole was treated using the empirical $(Z+1)^*$ approximation: i.e., the central absorbing C atom in the cluster is treated as a nitrogen atom with the electronic configuration, $1s^1 2s^2 2p^4$. The use of the core-hole approximation results in an increased intensity close to the absorption edge, giving better agreement with experiment. For the materials studied the core hole does not have a great influence, especially at the nonmetal edge. This is due to the high degree of screening of the core hole by the relatively free valence electrons, with a large weight on the nonmetal site, present in these conducting materials. Experimental broadening can be taken into account by varying the imaginary part V_{im} of the photoelectron energy, this being set, typically, to a constant value of 0.5 eV over the whole ELNES energy range. The main advantage of the real-space multiple-scattering technique over band-structure calculations is the ease with which nonperiodic systems may be modeled. Substoichiometric systems and structures containing vacancies may be examined with little extra effort or computing cost. The inclusion of approximations to account for the core hole produced during the excitation process is also relatively straightforward. One point to note concerning the multiple scattering method (specifically the calculation of phase shifts using MUFPOT) used here, is that the $X\alpha$ exchange potential (α is set to 0.8) used is independent of energy.[20] The exchange term, which accounts for the exchange correlation introduced by the Pauli exclusion principle is, however, known to be dependent on energy. The effect of this is to cause a deviation of the peak positions with energy compared with the experimental data and FLAPW results.

We have recently begun to investigate the real space MS code FEFF8.[21] Similar to the method described above, the scattering potentials are calculated by initially overlapping the free-atom densities within the muffin tin approximation [the muffin tins are overlapped by 15% to try and reduce the effects of potential discontinuities (Table I)]. However, in contrast to the ICXANES method, the phase shifts calculated within the FEFF8 package are based on a self-consistent-field calculation with a Hedin-Lundqvist exchange correlation potential which is energy dependent.[22] FEFF8 also differs from the ICXANES MS method in its treatment of multiple scattering within the cluster. FEFF8 does not divide the cluster into shells and treat intershell and intrashell scatterings separately; instead it solves for the relevant Green's function by direct inversion for all atoms in the cluster. FEFF8 is showing promising results, and these have been included in this paper to not only aid in the interpretation of the experimental data

but also to give a useful comparison between the two multiple scattering modeling methods.

The influence of the core hole on ELNES was approximated in all FEFF8 MS calculations via use of the Z^* approximation, i.e., the central C atom is given a $1s^1 2s^2 2p^3$ configuration. The differences in the models for the core hole used in the two multiple-scattering approaches probably reflects the differences in the calculation of the scattering phase shifts. $(Z+1)^*$ is an empirical, overapproximation used to account for deficiencies in the non-self-consistent phase shifts.[23] The FEFF8 MS calculations used identical clusters to those employed in the ICXANES MS calculations.

B. Full linearized plane augmented plane-wave method (FLAPW)

The electronic structure calculations were performed using the full linearized augmented plane-wave method using the package WIEN97.[24] The unit cell is separated into nonoverlapping atomic spheres and an interstitial region. The wave functions are described using radial solutions of Schrödinger's equation inside the spheres and plane waves in the interstitial regions. Exchange and correlation effects were treated using the generalized gradient approximation.[25] Unlike MUFPOT, no spherical average is taken inside the muffin-tin spheres nor volume average in the interstitial region. For each calculation, typically, 104 k points were used in the irreducible Brillouin zone (3000 k points in the whole cell), a maximum angular momentum for the radial wave functions ($l_{\max}$) of 12 and a plane-wave cutoff ($R_{\mathrm{MT}}K_{\mathrm{MAX}}$) of 8 or 9. Local orbitals were added to the basis set. This allows a better treatment of the problem of semicore states present in early transition metal compounds; semicore states are high lying, relatively extended core states (e.g., the Ti $3p$ states).[26] Also, addition of extra local orbitals, e.g., nonmetal s and p and metal d orbitals, at energies high above the Fermi energy, enables a better and more reliable description of the unoccupied states. Subsequently, we were able to obtain calculated absorption spectra extending up to 40 eV above the edge onset. To our knowledge, this is the first time such an accurate modeling has been achieved so far in energy above the Fermi level.

The nonmetal K-edge spectra were obtained by multiplying the respective p-DOS by their essentially atomic matrix elements. A 1.0-eV Lorentzian broadening function was then applied.

III. EXPERIMENT

Full details concerning the acquisition of the experimental EEL spectra presented in this paper have already been reported.[16] To summarize, the spectra were collected using a GATAN 666 parallel electron energy-loss spectrometer mounted on a VG Microscopes HB5 dedicated FEGSTEM with post-specimen lenses. The microscope was operated at 100 kV. Spectra were recorded with a dispersion of 0.1 eV per channel. The energy resolution, estimated from the full width at half maximum of the zero-loss peak, is approximately 0.3 eV. No attempt was made to deconvolute the plural scattering for the carbide spectra as they were recorded from very thin material. The spectra were acquired using a convergence semiangle of 11 mrad and a small collection semi-angle of 12.5 mrad, which implies that the dipole selection rule applies for the observed ELNES transitions. For the case of nonmetal K edges, this means that the excited electron is probing empty p-like states in the conduction band. For the metal $L_{2,3}$ edges, the empty d- and s-like states, weighted by the appropriate matrix elements, are probed, the d states being dominant.

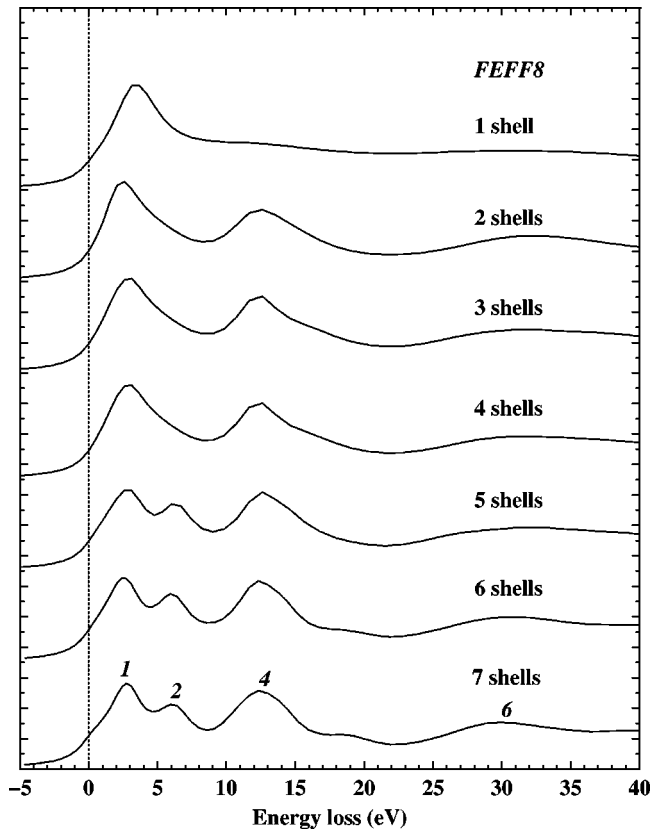

FIG. 1. Effect of increasing numbers of scattering shells for the FEFF8 MS calculation of the C K-ELNES of TiC.

IV. RESULTS AND DISCUSSION

A detailed comparison of both experimental and theoretical results are summarized graphically in Figs. 4–9.

A. Multiple scattering and FLAPW calculations of TiC carbon K-ELNES

A modeling of the near-edge structure using multiple-scattering methods is achieved by building a real-space cluster surrounding the central absorbing atom. The cluster is increased in size until the calculated spectra have fully converged. Figure 1 shows the effect of increasing the cluster size on the results of MS calculations for the C K edge in TiC calculated using the self-consistent FEFF8 method. The peak labeling scheme, shown in Fig. 4, follows that used by Pflüger *et al.*[27] and Craven and Garvie.[16] For both sets of MS results, convergence is achieved after addition of seven

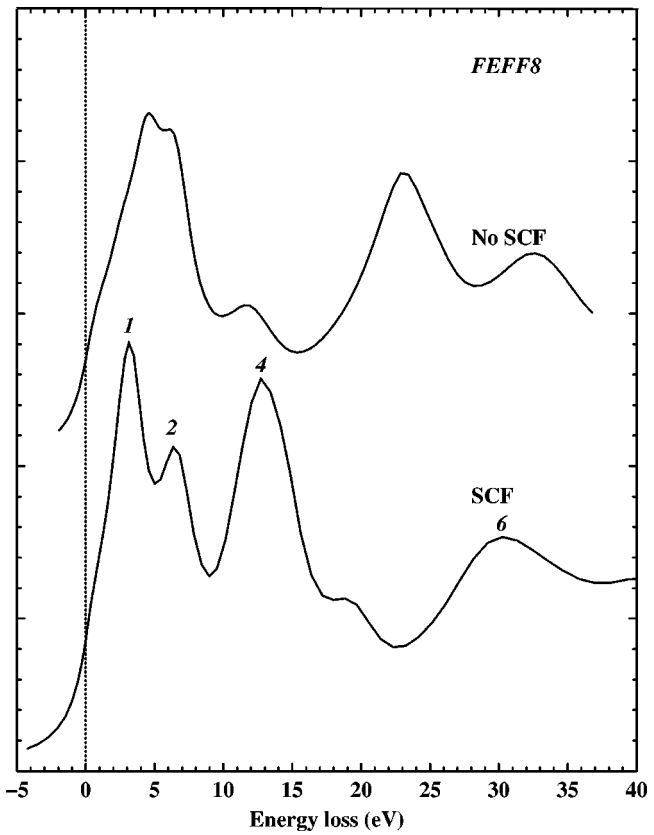

FIG. 2. Effect of self-consistency in the potential calculation on modeled C *K*-ELNES of TiC (FEFF8).

shells, this equating to a 93-atom cluster with a radius of approximately 0.6 nm. For TiC, the compositions of shells 1–7 are as follows: shell 1, 6 Ti; shell 2, 12 C; shell 3, 8 Ti; shell 4, 6 C; shell 5, 24 Ti; shell 6, 24 C; and shell 7, 12 C. The ICXANES MS results show a good correspondence with the FEFF8 MS results. However, there are some differences which are presumably due to the effects of self-consistency in the charge distribution, the different muffin-tin radii employed (and whether they overlap), the energy dependence of the exchange-correlation potential and, most probably, the different calculational algorithms employed in each case. Specifically in Fig. 2, we show the effects of including self-consistency for a fully converged calculation of the C *K*-ELNES in TiC using FEFF8, although these differences seem less dramatic than those observed using the non-self-consistent ICXANES code (Fig. 4), they do highlight the strong influence of charge redistribution on both peak intensities and peak positions observed in ELNES data. We discuss the magnitude of the charge redistribution later in the paper, where we consider the FLAPW band-structure results.

One advantage of the MS method is the ability to assign particular scattering events from different shells in the cluster to peaks in the ELNES data. Examination of Fig. 1 reveals that peak 1 is predominantly due to scattering from the first shell of six Ti atoms. Upon the addition of the second shell of 12 carbon atoms to the cluster, peaks 4 and 6 appear. Following the work of Rez *et al.*[28] and Kurata *et al.*[29] on the O *K*-ELNES of transition-metal oxides with the same NaCl-

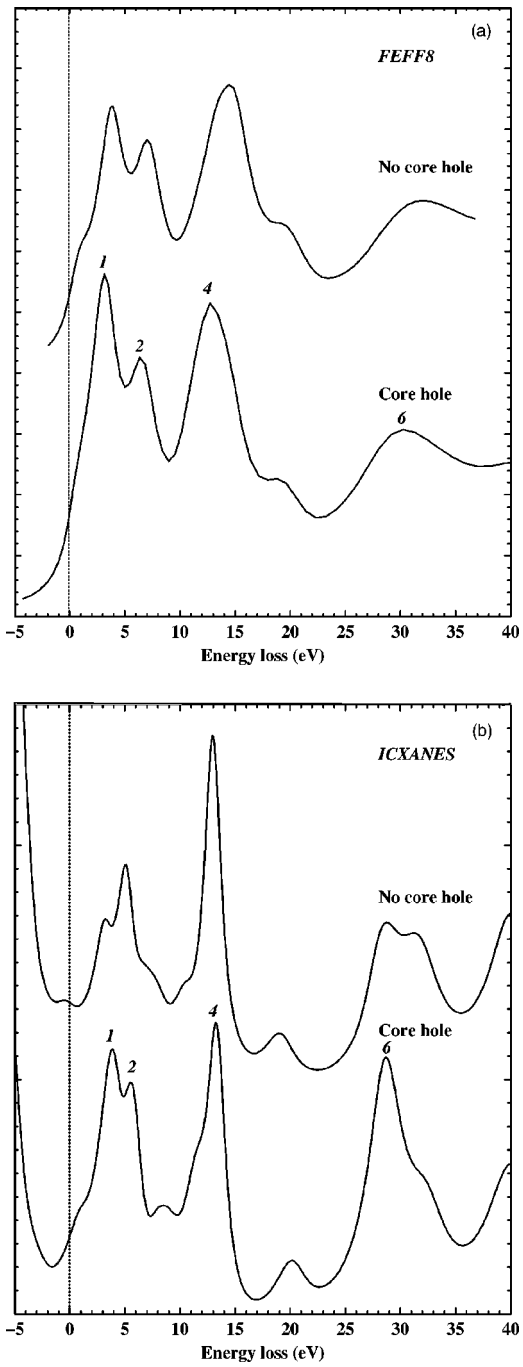

FIG. 3. Effect of the core hole approximation on the MS calculation of the C *K*-ELNES of TiC [(a) FEFF8, (b) ICXANES].

type structure, we conclude that peak 6 is due to intershell scattering from this first nonmetal shell while peak 4 is due to intrashell scattering within the same shell (shell 2). Further evidence of this conclusion is given later in the paper where we compare the nonmetal *K*-edge spectra of TiC, TiN, and TiO. The MS approach is also attractive in that it easily lends itself to the investigation of the effects of the core hole on the experimental spectra. As mentioned above, the effectively positive potential of the core hole tends to pull states down in energy, and so increase the intensity near the edge onset. This is clearly seen in Figs. 3(a) and 3(b) for the C

K-ELNES in TiC modeled using the FEFF8 and ICXANES codes. As the metal carbide materials under study have relatively high conductivities, the core hole tends to be screened from outer electrons, significantly lessening its impact on the spectra. This fact is supported by the FLAPW results, presented below, which show excellent agreement with the experimental data even though they are ground-state calculations. However, for insulating materials, it is extremely important to model the core hole correctly. For example, a strong effect may be seen on cation edges, especially for light elements, whereas the effect of the core hole on anion edges may be negligible. The degree of screening of the core hole also depends upon the degree to which the valence electrons are localized on the excited atom. In the TM carbides, the valence band is predominantly of C 2*p* character significantly reducing the effect of the core hole in inner-shell excitations from carbon sites.

The various steps in the FLAPW calculation are as follows: (a) Initially, the partial density of states of *p* character projected onto the carbon site was calculated using the self-consistent FLAPW procedure. (b) Next, the square of the dipole matrix elements, which are essentially atomiclike quantities, were calculated for the transitions from the C 1*s* level to the empty *p*-like states projected onto the carbon site. (c) The *p*-DOS and matrix elements were multiplied to produce the transition intensity. (d) This transition intensity was then broadened (typically by 1 eV) to take into account both the lifetimes of the initial and final states as well as instrumental effects such as overall energy resolution of the measurements. This produces the final broadened transition intensity which can be compared with ELNES data. A similar set of procedures also applies in the case of the MS calculations; however, here the *p*-DOS is calculated using scattering theory.

Figure 4 shows a direct comparison of the FLAPW results, both sets of MS results, and finally the experimental C *K*-edge spectrum for TiC. The FLAPW results are in excellent agreement with experiment, both in terms of peak positions and peak intensities, and these agree well with the MS calculations, particularly the self-consistent FEFF8 results. It is important to reiterate that the FLAPW calculations (unlike the MS calculations) do not include any approximation to account for the effect of the core hole; this is particularly evident in the relative intensity of peak 1 to peak 2, which is significantly lower than experimentally observed. The ICXANES MS results do include an approximation for the core hole, but lack self-consistency in the potential and this also leads to problems with relative peak intensities. The FEFF8 results, where both effects have been taken into account, appear to provide the most satisfactory agreement with experiment.

From a detailed study of the FLAPW results on TiC, we can divide the ELNES into two distinct regions; this is in line with previous band-structure calculations.[8] The region from 0 to 8 eV above the edge onset can be assigned to empty metal *d* orbitals (Ti 3*d*) hybridized with carbon 2*p* orbitals. The peak separation between peaks 1 and 2 can be viewed as a form of ''crystal-field splitting'' due to the octahedral coordination of titanium by carbon. For TiC, the measured separation is 2.2 eV. The region above 8 eV from the edge onset can be assigned to Ti 4*s* and 4*p* orbitals hybridized with C 2*p* orbitals.

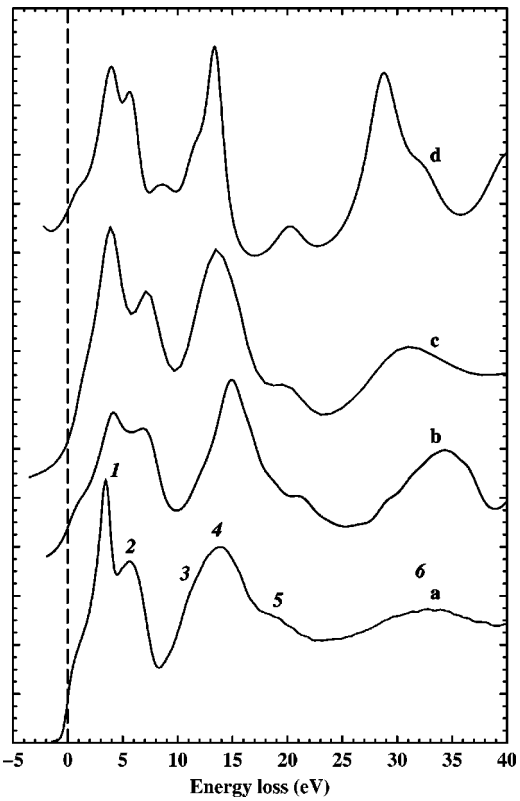

FIG. 4. Comparison of C *K*-edge spectra of TiC [(a) experimental, (b) FLAPW, (c) FEFF8, and (d) ICXANES].

B. Comparison of MS and FLAPW calculations with experimental carbide carbon *K*-ELNES

Figures 5–9 show a comparison of the FLAPW results, both sets of MS results, and the experimental data for the C *K*-ELNES in VC, ZrC, NbC, HfC, and TaC. Overall, the agreement between experiment and the theoretical results is good, especially for the FLAPW and, to a lesser extent, self-consistent MS calculations. In particular, the FEFF8 MS calculations show poor agreement with experiment for the case of TaC. The non-self-consistent MS calculations struggle to adequately model the spectra for the heavy element carbides, and this is also apparent to a lesser degree in the FEFF8 MS calculations.

For the 4*d* and 5*d* TM carbides, the experimental C *K*-ELNES spectra show a considerable amount of intensity and structure over the whole energy region between 0 and 15 eV above the edge onset, whereas the 3*d* TM carbides exhibit an intensity minimum between peaks 2 and 3 (roughly 8 eV above the edge onset). The lack of an intensity minimum in the C *K*-ELNES of the 4*d* and 5*d* carbides may be due to the more extended overlap of the TM 4*d* and 5*d* orbitals (relative to TM 3*d* for TiC and VC) with the C 2*p* orbitals, leading to the lack of a distinct division between the TM *d*- and the s*p*-hybridized regions as has been discussed for TiC in Sec. IV A. The ICXANES MS calculations for the

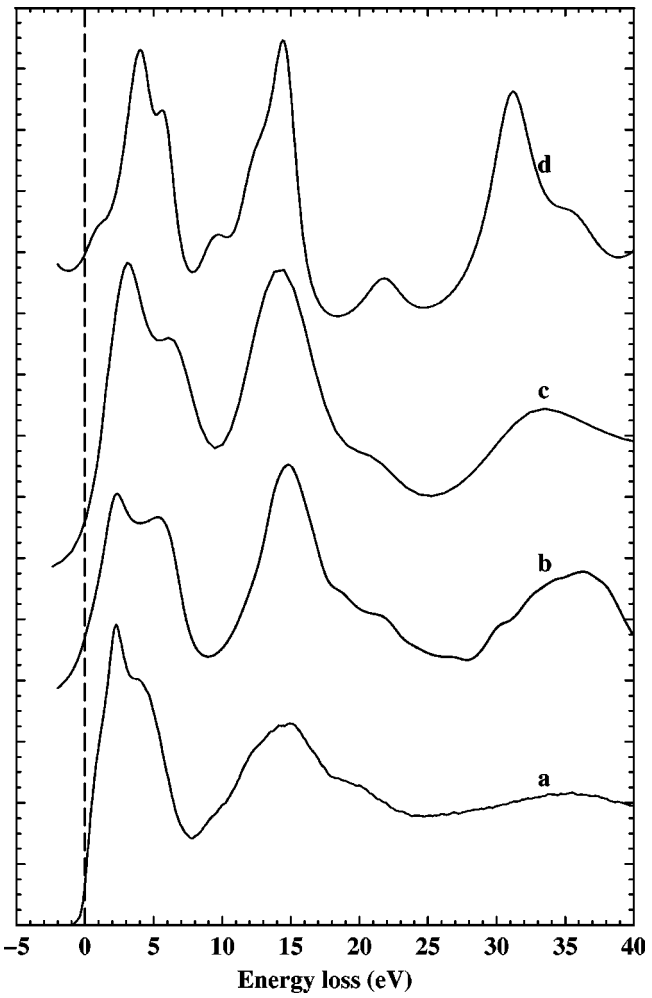

FIG. 5. Comparison of C *K*-edge spectra of VC [(a) experimental, (b) FLAPW, (c) FEFF8, and (d) ICXANES].

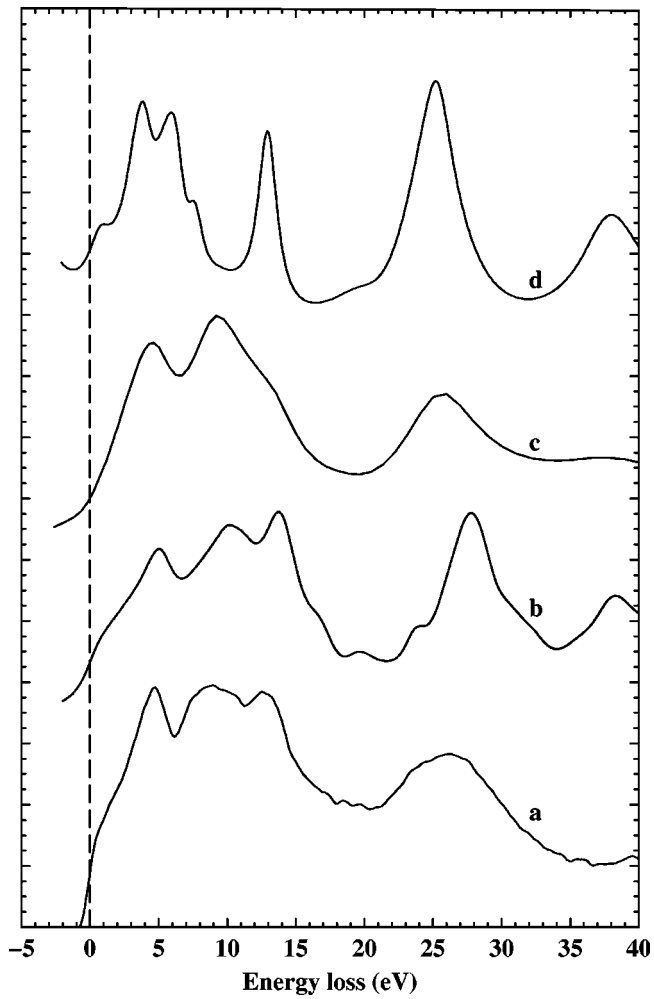

FIG. 6. Comparison of C *K*-edge spectra of ZrC [(a) experimental, (b) FLAPW, (c) FEFF8, and (d) ICXANES].

$4d$ and $5d$ TM carbides appear to be missing some of this intensity. As we will see, apart from NbC, the magnitude of ''charge transfer'' in this series of carbides is predicted to be similar; thus the discrepancies may, in part, be due to the spherical and volume averaging of the potential in the muffin tin based methods for the calculation of phase shifts employed in the MS methods. This may be a limitation for $4d$ and $5d$ TM carbides where the potential may possess increased directionality due to metal-metal interactions.

The current results also suggest that for higher atomic number TM carbides the effect of the core hole on the C *K*-edge of the carbides may be weaker as we go down the TM group and is perhaps overestimated by the approximations used in the MS calculations. Indeed, for HfC the agreement with experiment is marginally better for a calculation with no core hole.

A general trend in the data is that the MS methods consistently place the higher energy peaks (e.g., peak 6) at too low an energy relative to both the FLAPW method and experiment. This is discussed further in Sec. IV E. However, for the present we note that inclusion of the core hole in the MS methods will tend to reduce the energy of these features and, second, it may be the case that the less accurate MS methods have difficulty in describing accurately the energy positions of features near the edge onset and thus the corresponding alignment of the higher-energy features contains a systematic error.

Another noteworthy feature is that the peaks in the ICXANES MS calculations are all consistently too sharp which, in this method, may be a manifestation of the division of the scattering into intershell and intrashell components within the cluster. Multiple intershell scattering would be expected to lead to a sharpening of these resonances.

General trends observed in the experimental C *K*-ELNES of the series of TM carbides were already discussed by Craven and Garvie,[16] and, on going from the $3d$ to $4d$ to $5d$ TM carbides, these involve (a) an increase in absolute energy of peak 1, and (b) a decrease in the energy separation between peaks 1 and 4. This second systematic change is modeled extremely well by the FLAPW calculations.

The success of the FLAPW ground-state calculations confirms the high degree of screening of the core hole from the unoccupied states during the EELS excitation process. To account for the core hole within the FLAPW method, we envisaged requiring a large$(2\times2\times2)$ supercell (64 atoms, and a core-hole–core-hole distance of 0.8656 nm) sufficient

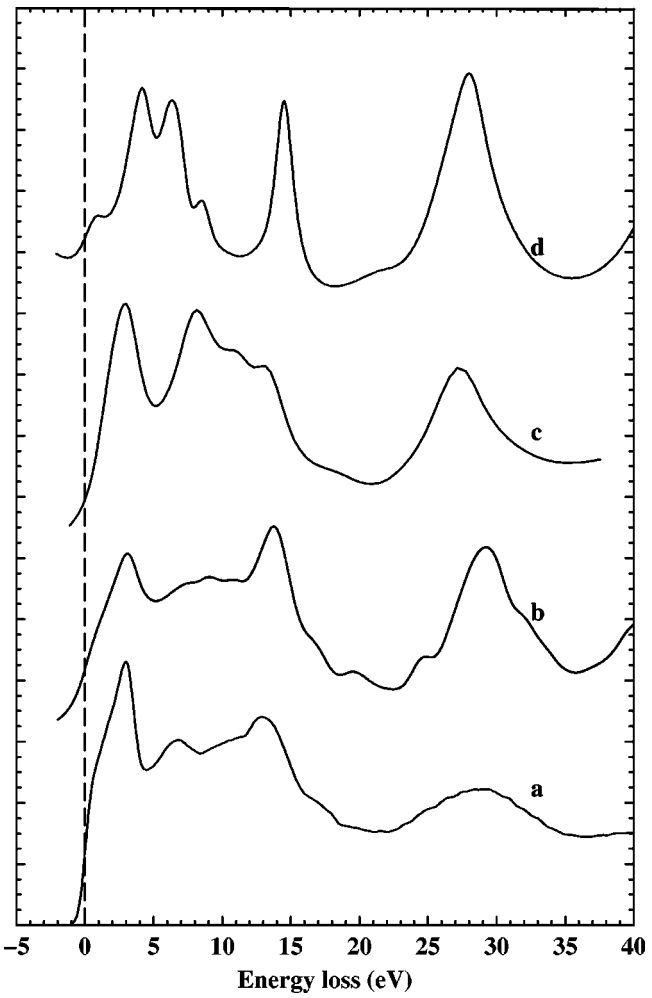

FIG. 7. Comparison of C *K*-edge spectra of NbC [(a) experimental, (b) FLAPW, (c) FEFF8, and (d) ICXANES].

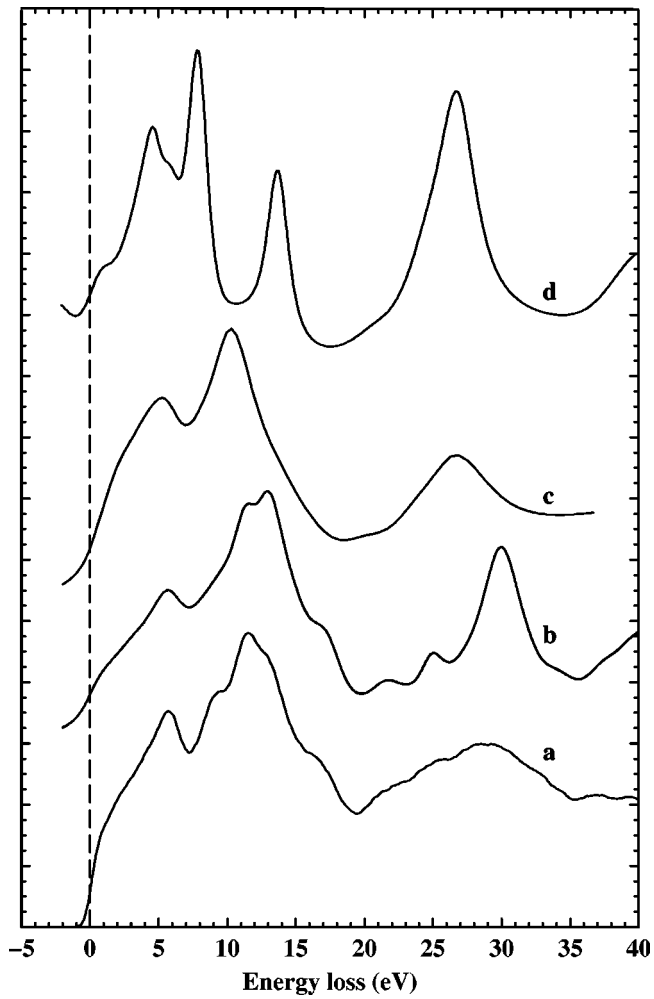

FIG. 8. Comparison of C *K*-edge spectra of HfC [(a) experimental, (b) FLAPW, (c) FEFF8, and (d) ICXANES].

to avoid possible interaction between neighboring core holes. This would have been prohibitive in terms of computing cost. However, the recent work of Paxton, who has performed linear muffin tin orbital calculations on TiC, indicated that a primitive cell (eight atoms, and a core-hole–core-hole distance of 0.4328 nm) would suffice.[30] Though taking significantly longer than the ground state (fcc) calculations, with access to parallel processing facilities they were readily accomplished. The core hole on the absorbing carbon atom was accounted for using the Z^* approximation, i.e., an electron from the 1*s* orbital from removed and placed in the valence band. Figures 10 and 11 compare the experimental C *K*-ELNES of TiC and ZrC respectively with the FLAPW calculations for the ground state and excited state (core-hole-approximated) structures. As expected, the differences between the ground- and excited-state calculations are not dramatic. However, accounting for the core hole is manifested in a movement of states down toward the edge onset, giving a superior match of the peak energies and intensities.

C. Relative effectiveness of the two modeling approaches

We shall now draw some general conclusions regarding the relative merits of the three approaches to modeling the transition metal carbide *K* edges. It is clearly seen from Figs. 5–9 that the FLAPW calculations are consistently in agreement with the experimental data. They reproduce all the significant peaks with accurate peak energies and intensities. We have shown that for TiC and ZrC the presence of the core hole may be modeled successfully using the FLAPW method, albeit with a significant increase in computing cost. As the effect of the core hole upon the C *K*-ELNES of these materials is small, we are able to successfully model the experimental data with ground state FLAPW calculations (an advantage of the ICXANES and FEFF8 MS methods is that approximations for the effect of the core hole may be made with no increase in calculation time). With the rapidly increasing speed and affordability of powerful multiprocessor machines, we envisage that periodic supercell calculations to account for the core hole will become common place within the coming years.

We have performed MS calculations using the established MUFPOT/ICXANES and the more recent FEFF8 codes. We feel that the calculation of the potential self-consistently within the FEFF8 code gives it major advantage for accurate ELNES modeling. We see in Sec. IV G that charge transfer is taking place from the metal to the nonmetal. Though both codes

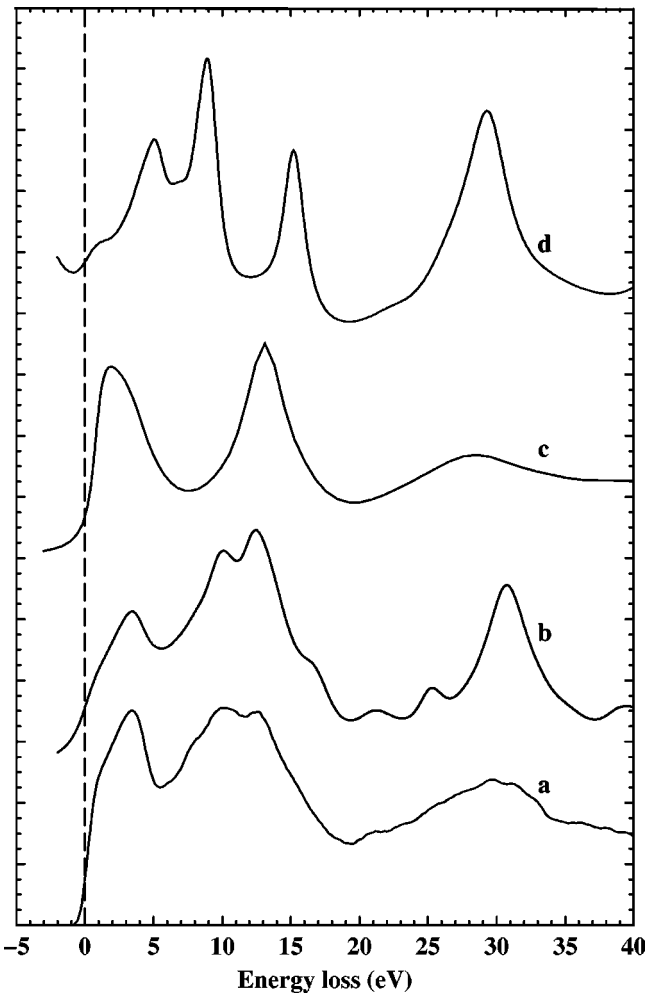

FIG. 9. Comparison of C *K*-edge spectra of TaC [(a) experimental, (b) FLAPW, (c) FEFF8, and (d) ICXANES].

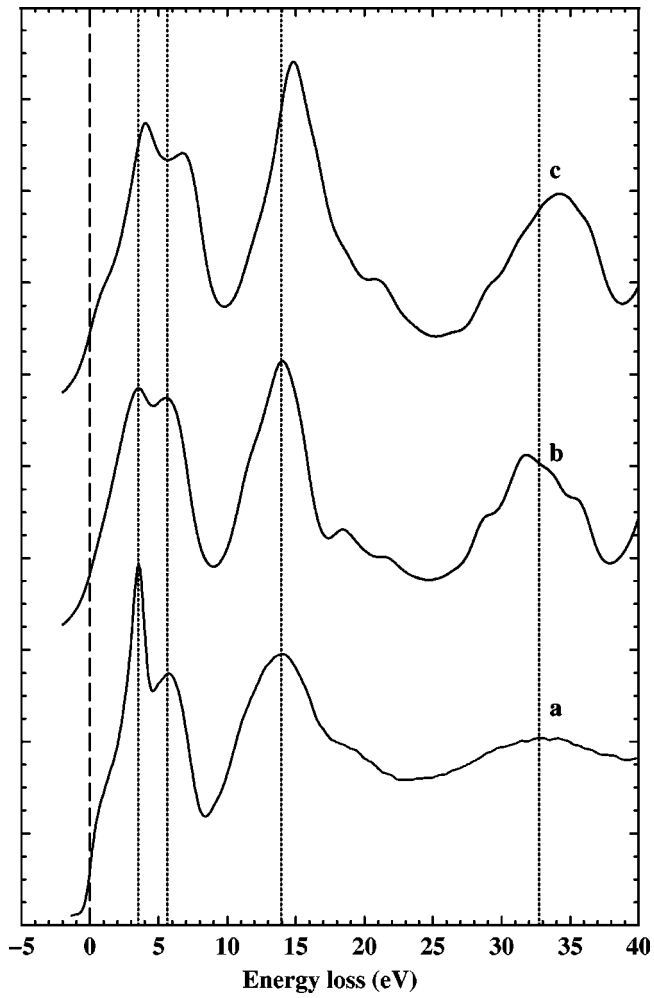

FIG. 10. C *K*-edge spectra of TiC calculated using the FLAPW method [(a) experimental; (b) core-hole correction, primitive unit cell; and (c) ground-state calculation, fcc cell].

model the first-row TM carbides well, as we descend the groups we see the advantage that self consistency brings to maintaining the desired accuracy in modeling of the experimental spectra. Further investigation and refinement in the running of the FEFF8 code will be undertaken in a future publication.

D. Influence of lattice parameter on carbide C *K*-ELNES

Since all the carbides are isostructural, the main variations within the range of carbides studied are the effect of changing the metal atom and the effect of changing the lattice parameter. To separate these two effects, we initially keep things simple and artificially adjust the lattice parameter in the calculations. The lattice parameter of TiC was varied between + and −5% of its experimental value, demonstrating a significant influence upon the ELNES peak positions. The peaks systematically move toward the edge onset as the lattice parameter increases; the degree of shift increases with the energy of the peak above the threshold. This effect was noted by Natoli,[31] whereby certain peak positions in the near-edge structure may be influenced by the radial distance to the local coordination shells. These distances are directly related to the lattice parameter of the compound. In a scattering description, such events may be termed coordination shell multiple-scattering resonances (MSR's) and may be analyzed using a simple EXAFS/extended electron energy loss fine structure-type analysis (the latter being based on a single scattering description).

If a particular ELNES feature may be identified as a scattering resonance, then it can be shown[32] that

$$\Delta E = \frac{\hbar}{8m} \frac{[(2n+1)\pi - \phi(k)]^2}{\alpha_i^2} \frac{1}{a^2}, \tag{1}$$

where ΔE is the peak position above threshold, $\phi(k)$ is a phase shift from the relevant coordination shell, and α_i is the distance to the *i*th shell of neighbors in units of the lattice parameter *a*, and *n* is an integer. Thus the above analysis predicts ΔE to vary linearly with $1/a^2$ with the straight line passing through the origin, assuming that $\phi(k)$ does not vary significantly with energy.

The data for peak 6 are the closest to passing through the origin. Our previous analysis (Sec. IV A) associated peak 6 with intershell scattering from the second shell surrounding the absorbing carbon atom (i.e., the first carbon shell). The

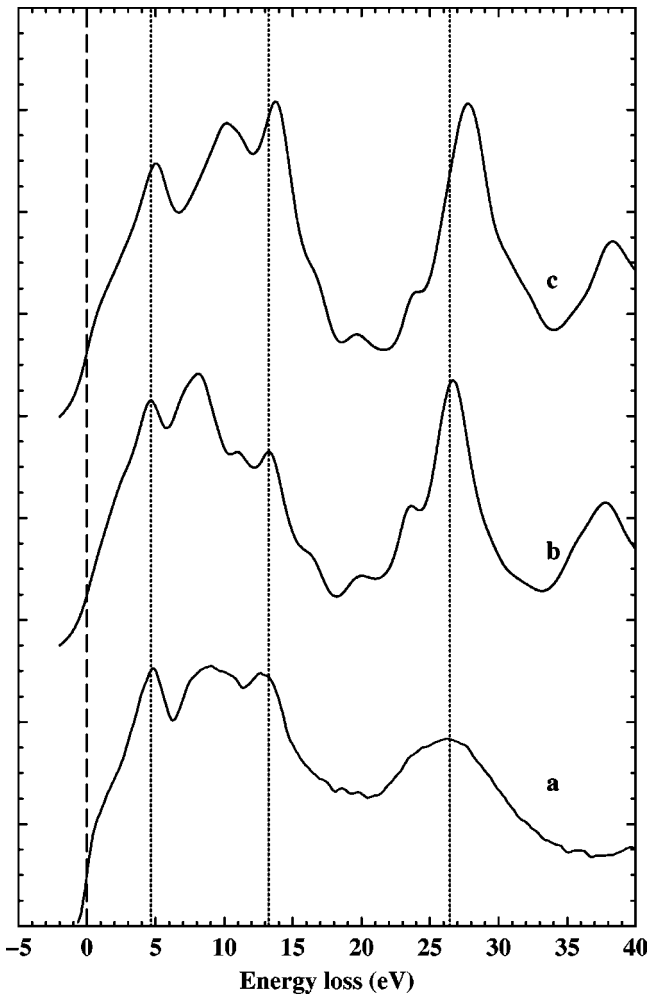

FIG. 11. C *K*-edge spectra of ZrC calculated using the FLAPW method [(a) experimental; (b) core-hole correction, primitive unit cell; and (c) ground-state calculation, fcc cell].

dependence of ΔE on variations in $1/a^2$ for the other peaks (1–5) shows differing slopes and intercepts. It is envisaged that there is a strong intrashell scattering component in their origin, as suggested in Fig. 1.

E. Influence of lattice parameter and metal atom

Increasing the complexity of the analysis, we now consider the effects of the combined variation of both the lattice parameter and the metal atom on the C *K*-ELNES via a detailed consideration of our group-IVA and -VA data. Plots of the peak energy above the edge onset (ΔE) versus $1/a^2$ for the experimental C *K*-edge data of the TM carbides may be found in Craven and Garvie.[32] Straight line graphs are obtained for peaks 1, 2, 4, and 6; however, as alluded to in Sec. IV D, only peak 6 gives a positive slope passing through the origin which is presumably due to it being associated with a multiple-scattering resonance from the first nonmetal shell. A comparison of the ΔE versus $1/a^2$ plots for peak 6, determined experimentally and from the three sets of calculated C *K*-ELNES (FLAPW, FEFF8 MS, and ICXANES MS), show the FLAPW results to be closest to experiment; the self-consistent MS (FEFF8) results also show good agreement.

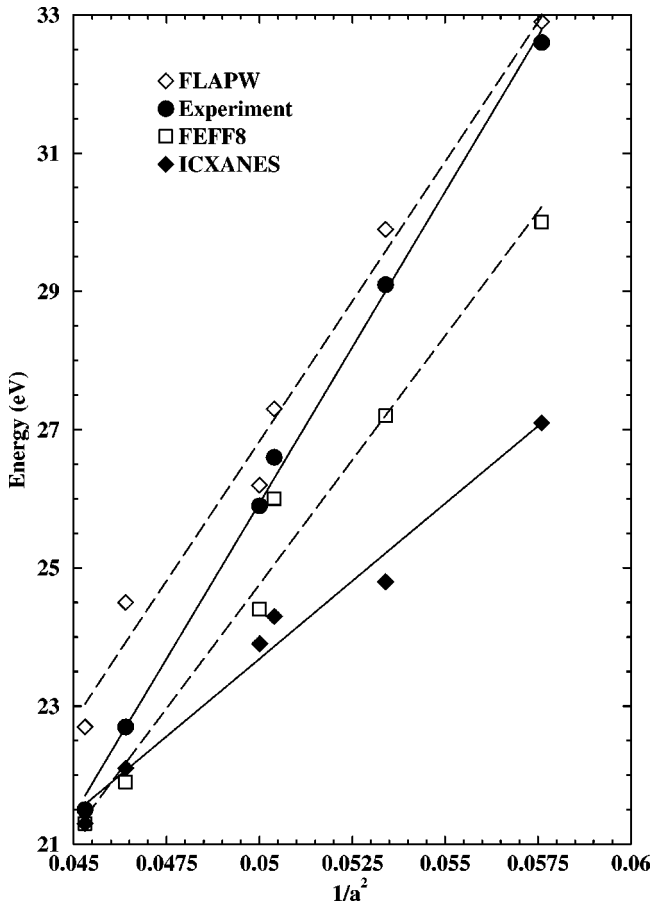

FIG. 12. Plot of the energy difference between peaks 1 and 6 against $1/a^2$ for transition-metal carbides: experimental and modeled data.

Some confusion exists as to whether the peak positions of scattering resonances should be measured relative to the edge onset, the conduction-band onset (not necessarily the same quantity as the apparent edge onset due to the effect of the core hole), or the Fermi level (which would require some additional information such as x-ray photoelectron spectroscopy binding energies and the band gap). In order to circumvent this problem one method is to measure peak separations. Figure 12 shows the energy difference between peaks 6 and 1 plotted against $1/a^2$ for both the experimental and calculated C *K*-ELNES data. It can be seen that the FLAPW results show best agreement with experiment, while the FEFF8 results are considerably superior to the ICXANES results. The separation of peaks 1 and 6 can be seen to be a potentially sensitive measure of the lattice parameter of these materials, this information being available on the nanometer scale through the use of modern TEM's/STEM's.

F. Influence of nonmetal atom on nonmetal *K*-ELNES

Figure 13 shows a comparison between the theoretical nonmetal *K* edges of TiC, TiN, and TiO calculated using the FLAPW method. The calculations for TiN and TiO show good agreement with the N *K*- and O *K*-ELNES obtained from these materials.[32,33]

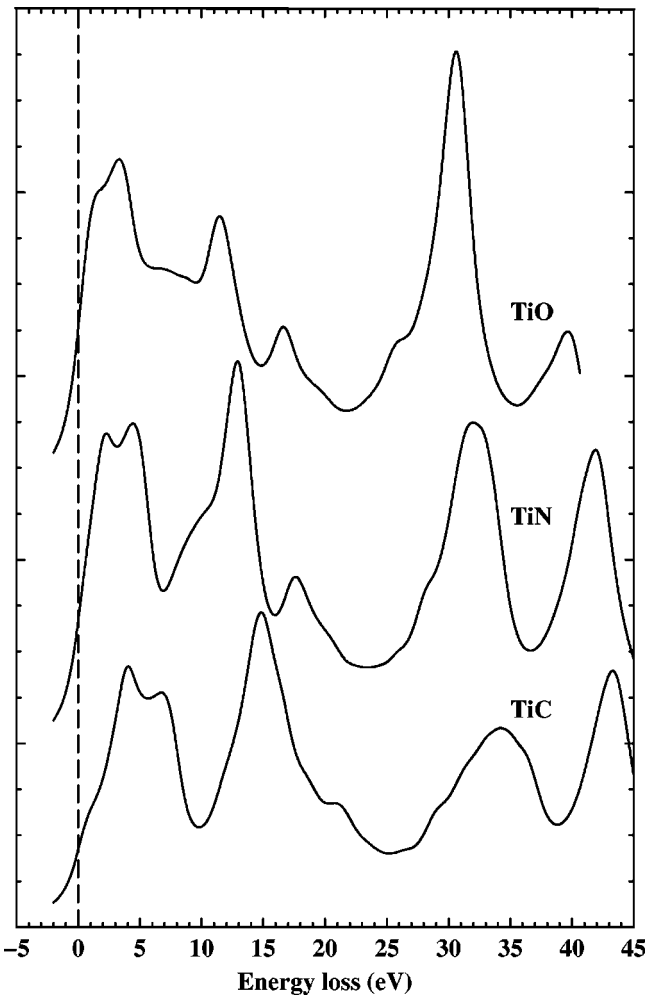

FIG. 13. Comparison of the theoretical nonmetal *K* edges of TiC, TiN, and TiO calculated using the FLAPW method.

As all three compounds are isostructural, the main variations between TiC, TiN and TiO are (a) a change in lattice parameter and hence resonance distance for MSR's and (b) a change in the nonmetal atom and hence backscattering phase shift for the MSR associated with peak 6 which is associated with the first nonmetal shell.

From the work shown in Sec. IV D, we may expect that the experimentally observed decrease in lattice parameter from TiC ($a=0.4328$ nm) through TiN ($a=0.4241$) to TiO ($a=0.4176$) to be reflected in the movement of the peaks 1–6 away from the edge onset in the nonmetal *K*-ELNES. However, the opposite effect is observed here (Fig. 13), and also in the experimental ELNES. This anomaly must be due to differences in the backscattering phase shifts of the nonmetal atoms. Plotting the phase shifts ϕ for carbon, nitrogen, and oxygen atoms in the cluster as a function of energy, we observe a progressive increase in the magnitude of the phase shift as the atomic number increases. This results in a decrease in the numerator in Eq. (1) as the atomic number of the backscattering shell increases, leading to the experimentally observed decrease in ΔE. This change in the backscattering phase shift also directly affects the relative intensity of MSR's involving nonmetal coordination shells, e.g., peak 6. The electron backscattering power of an atom is known to increase with its electronegativity, which explains the increase in the relative intensity of peak 6 (e.g., the peak 6:peak 1 intensity ratio) as the second shell changes from C, through N, to O.

A further change in going from TiC, through TiN to TiO, is an increase in the number of valence electrons from 8 to 10. In terms of a rigid band model, this shifts the Fermi level to higher energies causing the observed loss in intensity of peak 1.

As mentioned in Sec. IV A, peaks 1 and 2 in the nonmetal (NM) ELNES reflect the hybridization between the TM $3d$ and nonmetal $2p$ orbital. The energy difference (crystal-field splitting) between peaks 1 and 2, observed at the nonmetal *K* edge, decreases from TiC, through TiN, to TiO. This TM $3d$–NM $2p$ hybridization should also be apparent at the TM L_3 and L_2 edges. Figure 14 compares theoretical Ti L_3 edges and nonmetal *K* edges for TiC, TiN, and TiO calculated using the FLAPW code WIEN97. The features corresponding to peaks 1 and 2 observed at the nonmetal *K* edges are clearly reflected in the metal L_3 edges. Further comparison of these results with experimental metal $L_{2,3}$ ELNES data will be made in a forthcoming publication,[34] as will a complete set of experimental and theoretical data for the TM nitrides.

G. Charge transfer

Next we address the subject of charge transfer in these materials. As noted in Sec. IV A, it appears that proper consideration of the exact self-consistent charge distribution is essential if accurate agreement with experiment is to be achieved via MS modeling of the C *K*- and N *K*-ELNES.

With this in mind, we have investigated the degree of charge transfer present in the TM carbides using the FLAPW method. Charge transfer is a very ill-defined concept, and depends critically on an exact division of the volume within the unit cell. However, for the purposes of this study we take it to be the difference in the total charge within each muffin tin sphere (and the interstitial region), between the final step in the self-consistency cycle (i.e., the self-consistent charge distribution) and the initial step in the cycle (i.e., simply the superposition of neutral atomic potentials). This is similar to the definition employed by Lie *et al.*,[35] and essentially represents the movement of charge to or from muffin-tin (MT) volumes (which to some extent are somewhat arbitrary) from the initial neutral atom values during the achievement of self consistency in terms of total energy.

These results are presented in Table II. For all materials studied, the charge transfer is into the nonmetal MT sphere, and lies in the range 0.25–0.33 electrons, which is relatively small compared to any description in terms of formal charges. This transfer of electrons to the nonmetal is generally balanced by a corresponding reduction in charge on the TM site (apart from slightly anomalous results for the Nb compounds), with little charge entering the interstitial region.

Thus it would appear that, although the degree of charge transfer in the final self-consistent charge distribution is small relative to the neutral atom values, it does make a

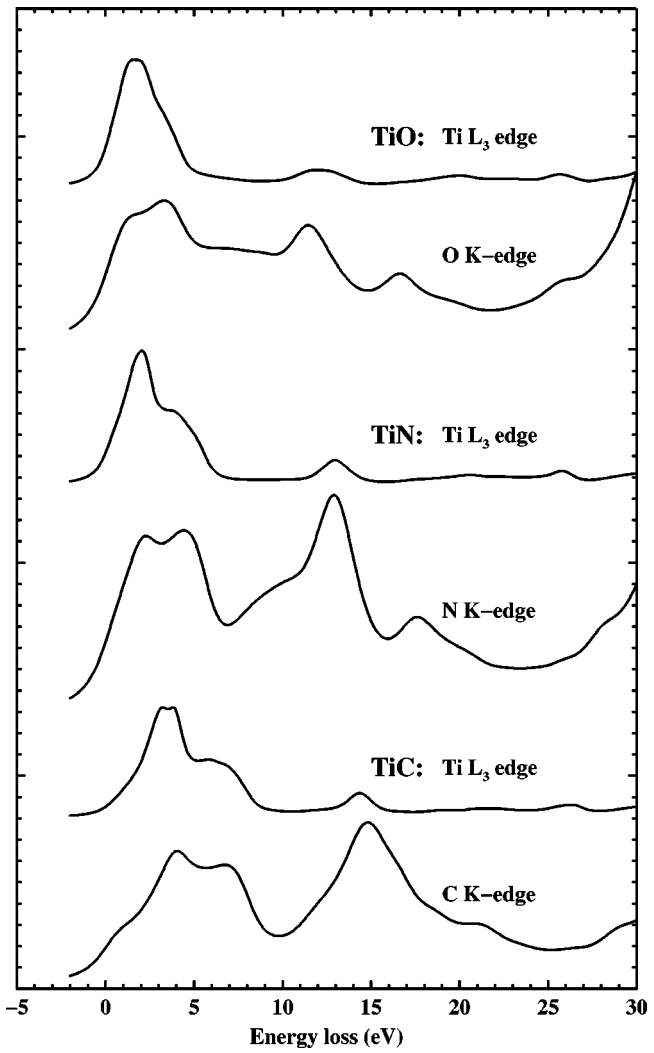

FIG. 14. Comparison of the metal L_3- and nonmetal K-edge spectra for TiC, TiN, and TiO (FLAPW).

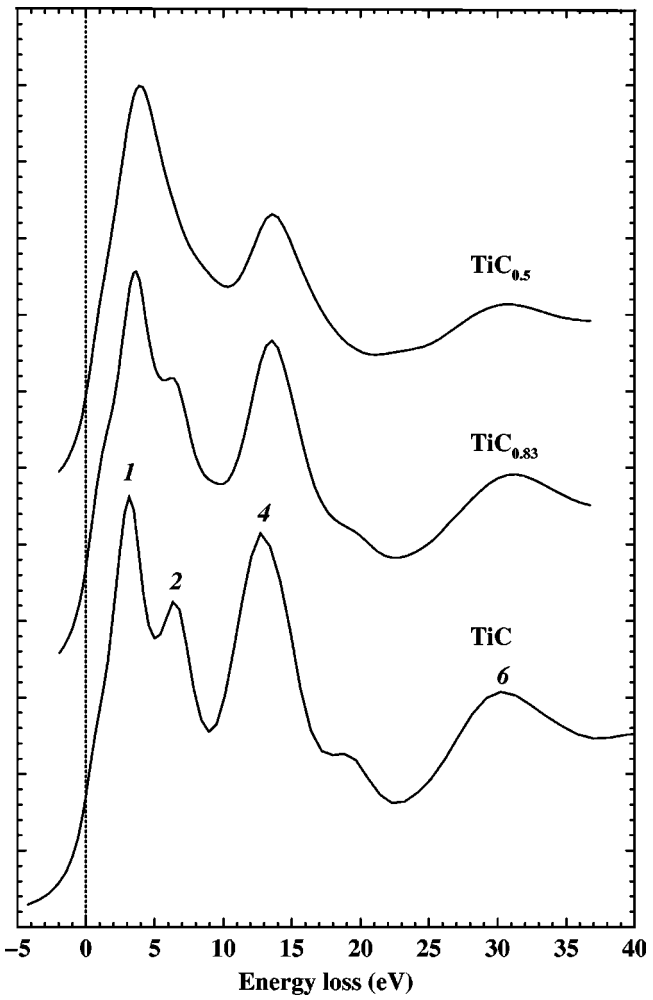

FIG. 15. Theoretical C K-edge spectra (FEFF8) of TiC_x showing the effect of metal and nonmetal stoichiometries.

significant impact on the MS modeling procedure. However, it is important to stress the validity of the assumption of the previously employed in the majority of MS phase-shift calculations that, in the absence of a fully consistent potential calculation, the best approximation is a simple superposition of neutral atom potentials rather than the assumption of any formal charges on atomic species.[36,37] In other words, the final self-consistent potential in a solid is approximated well by a superposition of neutral atom potentials provided a sensible choice of MT radii are chosen.

TABLE II. Muffin-tin radii (a.u.) employed for the FLAPW calculations of the TM carbides and the derived charge transfer (electrons) data.

	M (a.u.)	C (a.u.)	M (e^-1)	C (e^-1)	Interstitial (e^-1)
TiC	1.90	1.80	−0.25	+0.26	−0.01
VC	1.90	1.80	−0.25	+0.25	0.00
ZrC	2.00	1.80	−0.23	+0.27	−0.08
NbC	1.90	1.80	−0.44	+0.33	+0.11
HfC	2.00	1.80	−0.25	+0.29	−0.04
TaC	1.90	1.80	−0.28	+0.30	−0.02

H. Influence of nonstoichiometry

Transition-metal carbides can exhibit a range of stoichiometries. Figure 15 shows the effect of nonstoichiometry in the TiC structure on the C K-ELNES, as calculated by the FEFF8 MS method. Carbon vacancies were randomly removed from the cluster so as to simulate TiC_x, where x equals 0.5, 0.83, and 1.0. We have not included any effects of relaxation in atom positions due to the presence of vacancies. The C vacancies create nonequivalent C and Ti atom sites, however, repeated calculations revealed that a cluster containing random C vacancies represents a good approximation for the calculation of the averaged C K-ELNES which would be measured experimentally.

For the range of stoichiometries chosen here, there is less than a 1% difference in lattice parameter;[38] thus we observe that peak energies are unchanged for $x=0.5$, 0.83, and 1.0.

However, changes in the relative peak intensities are clearly apparent, which reflects the influence on the scattering induced by the presence of vacancies. In particular, the intensity of peak 4 is strongly affected as it arises from intrashell multiple scattering within the first carbon shell.

The intensities of peaks 2, 4, and 6 are strongly affected, as well as the energy separation between peaks 1 and 2. As discussed in Sec. IV A, peaks 6 and 4 are due to intershell and intrashell scattering involving the first carbon shell; hence it is to be expected that any reduction in carbon content within the cluster would lead to reduced scattering and hence reduced peak intensities.

The main trends predicted by the MS modeled C *K*-ELNES as a function of nonstoichiometry are in good agreement with the experimental results of Pflüger *et al.*[27] Here, as TiC_x became increasingly carbon deficient, they observed a decrease in the relative intensities of peaks 2 and 4 (their data only extend some 30 eV above the edge onset, and therefore do not include peak 6) as well as a reduction in the separation between peaks 1 and 2.

V. CONCLUSIONS

This work has provided a comprehensive review and comparison of ELNES modeling procedures as applied to the TM carbides of groups IVA and VA, possessing a NaCl structure. Excellent agreement with experimental C *K*-ELNES has been achieved particularly with the FLAPW code, WIEN97, even up to 40 eV above the edge onset. Multiple-scattering methods have been shown to be useful especially when one considers their flexibility and relatively quick calculational times compared with band-structure methods. Consideration of the effects of self-consistency in terms of the charge distribution, the inclusion of an adequately large basis set, and the influence of the core hole have all been included.

We have identified the effects that changes in lattice parameter and composition have upon the ELNES, thus enabling the extraction of useful information from these complicated edge structures. Future work will study the mutual solubility of transition-metal carbides and nitrides. We will investigate changes in the ELNES for such mixed TM carbides/nitrides and TM carbonitride compounds.[34]

It should be noted that we recently performed modeling upon the group-IVA and -VA transition-metal nitrides. All are isostructural with the TM carbides, except TaN which has a hexagonal structure. Very similar trends are observed to those found in the transition-metal carbide data. Again, the most successful modeling method was found to be the FLAPW code, WIEN97, with excellent agreement at energies high above the absorption edge. Space precludes us from including the results or discussion here. However, further details are available from the authors and may be found in a future publication.

ACKNOWLEDGMENTS

The authors are grateful to Dr. Knut Lie (NTNU, Trondheim) and Dr. Peter Blaha (Vienna University of Technology) for valuable advice concerning the WIEN97 band structure calculations, and to the EPSRC (Grant Nos. GR/K93600, GR/L06850, and GR/L52956) for funding. Extremely constructive comments of a reviewer are also greatly appreciated.

[1] L. E. Toth, *Transition Metal Carbides and Nitrides* (Academic Press, New York, 1971).
[2] J. P. Landesman, G. Treglia, P. Turchi, and F. Ducastelle, J. Phys. (France) **46**, 1001 (1985).
[3] H. Holleck and V. Schier, Surf. Coat. Technol. **76**, 328 (1995).
[4] W. D. Sproul, Science **273**, 889 (1996).
[5] T. Gladman, *The Physical Metallurgy of Microalloyed Steels* (Institute of Materials, London, 1997).
[6] R. F. Egerton, *Electron Energy Loss Spectroscopy in the Electron Microscope*, 2nd ed. (Plenum Press, New York, 1996).
[7] J. Bruley, V. J. Keast, and D. B. Williams, J. Phys. D **29**, 1730 (1996).
[8] R. Ahuja, O. Eriksson, J. M. Wills, and B. Johansson, Phys. Rev. B **53**, 3072 (1996).
[9] A. H. Cotrell, *Chemical Bonding in Transition Metal Carbides* (Institute of Materials, London, 1995).
[10] D. L. Price, B. R. Cooper, and J. M. Wills, Phys. Rev. B **46**, 11 368 (1992).
[11] V. P. Zhukov, V. A. Gubanov, O. Jepsen, N. E. Christensen, and O. K. Andersen, J. Phys. Chem. Solids **49**, 841 (1988).
[12] A. Neckel, P. Rastl, R. Eibler, P. Weinberger, and K. Schwarz, J. Phys. C **9**, 579 (1976).
[13] G. H. Schadler, A. M. Boring, P. Weinberger, and A. Gonis, Phys. Rev. B **38**, 9538 (1988).
[14] P. Marksteiner, P. Weinberger, A. Neckel, R. Zeller, and P. H. Dederichs, Phys. Rev. B **33**, 812 (1986).
[15] P. Marksteiner, P. Weinberger, A. Neckel, R. Zeller, and P. H. Dederichs, Phys. Rev. B **33**, 6709 (1986).
[16] A. J. Craven and L. A. J. Garvie, Microsc. Microanal. Microstruct. **6**, 89 (1995).
[17] P. J. Durham, J. B. Pendry, and C. H. Hodges, Comput. Phys. Commun. **25**, 193 (1982).
[18] D. D. Vvedensky, D. K. Saldin, and J. B. Pendry, Comput. Phys. Commun. **40**, 421 (1986).
[19] J. B. Pendry, *Low Energy Electron Diffraction* (Academic, London, 1974).
[20] M. Vaarkamp, I. Dring, R. J. Oldman, E. A. Stern, and D. C. Koningsberger, Phys. Rev. B **50**, 7872 (1994).
[21] A. L. Ankudinov, B. Ravel, J. J. Rehr, and S. D. Conradson, Phys. Rev. B **58**, 7565 (1998).
[22] L. Hedin and S. Lundqvist, Solid State Phys. **23**, 1 (1969).
[23] R. Brydson, D. D. Vvedensky, W. Engel, H. Sauer, B. G. Williams, E. Zeitler, and J. M. Thomas, J. Phys. Chem. **92**, 962 (1988).
[24] P. Blaha, K. Schwarz, P. Sorantin, and S. B. Trickey, Comput. Phys. Commun. **59**, 399 (1990).
[25] J. P. Perdew, S. Burke, and M. Ernzerhof, Phys. Rev. Lett. **76**, 3865 (1996).

[26] D. Singh, *Plane Waves, Pseudopotentials and the LAPW Method* (Kluwer, Dordrecht, 1994).
[27] J. Pfluger, J. Fink, G. Crecelius, K. P. Bohnen, and H. Winter, Solid State Commun. **44**, 489 (1982).
[28] P. Rez, X. Weng, and H. Ma, Microsc. Microanal. Microstruct. **2**, 143 (1991).
[29] H. Kurata, E. Lefvère, C. Colliex, and R. Brydson, Phys. Rev. B **47**, 13 763 (1993).
[30] A. T. Paxton, M. van Schilfaarde, M. Mackenzie, and A. J. Craven, J. Phys.: Condens. Matter **12**, 729 (2000).
[31] C. R. Natoli, *EXAFS and Near-Edge Structure*, Springer Series in Chemical Physics Vol. 27 (Springer-Verlag, Berlin, 1983), p. 43.
[32] A. J. Craven, J. Microsc. **180**, 250 (1995).
[33] M. S. M. Saifullah, C. B. Boothroyd, G. A. Botton, and C. J. Humphreys, Inst. Phys. Conf. Ser. **153**, 167 (1997).
[34] M. MacKenzie, A. J. Scott, A. J. Craven, and R. Brydson (unpublished).
[35] K. Lie, R. Høier, and R. Brydson, Phys. Rev. B **61**, 1786 (2000).
[36] D. G. McCulloch and R. Brydson, J. Phys.: Condens. Matter **8**, 3855 (1996).
[37] X. Weng and P. Rez, Phys. Rev. B **39**, 7405 (1989).
[38] M. Guemmaz, G. Moraitis, A. Mosser, M. A. Khan, and J. C. Parlebas, J. Phys.: Condens. Matter **9**, 8453 (1997).